Analysis and research on teeth thermodynamic coupling contact of gear transmission system

Xigui Wang[1,2], Yongmei Wang[3], Xuezeng Zhao[*1] and Xinglin Li[4]

[1]*Mechatronics school, Harbin Institute of Technology, Harbin 150001, China*
[2]*703 Research of Institute, Harbin 150078, China*
[3]*Motorcar Engineering, Heilongjiang Institute of Technology, Harbin 150036, China*
[4]*Hangzhou Bearing Test and Research Center, Hangzhou 310022, China*

Abstract. In the gear meshing process, gear temperature field concerns the meshing surface friction, the friction heat depends on the contact pressure, the contact pressure is affected by the elastic deformation of gears and the temperature field caused by the thermal deformation, so the temperature field, stress field and displacement field should be mutual coupling. It is necessary to consider in meshing gear pair in the operation process of thermodynamic coupling contact stress (TCCS) and thermodynamic coupling deformation (TCD), and based on thermodynamic coupling analysis (TCA) of gear teeth deformation.

Keywords: gear; temperature field; TCCS; TCD; TCA

1. Introduction

Gear transmission is a kind of constant power transmission relying on the teeth surface meshing to transmit motion and power (Zhang *et al.* 2006, Kim *et al.* 2007, Nikas 2010, Yang *et al.* 2009 Czichos 2010, De Mello *et al.* 2009). In gear running process, influence of alternate meshing arising teeth load distribution and impact, the teeth surface contact stress appears uneven distribution, which is one of main factors determining the level of gear teeth temperature (Gayathri 2012, Radhika 2014, Rout 2007, Wilke *et al.* 2011, Escobar Galindo 2009). In addition, thermal-elastic deformation caused by gear meshing will make teeth profile curve deviates from the standard involute, resulting appears strong shock and vibration in gear system (Hammes et al. 2014, De Mello *et al.* 2013, Silverio *et al.* 2011, Hanesch 2009, Mironova-Ulmane 2007, Efremov *et al.* 2008).

Although the size and distribution of teeth surface contact stress will directly affect the meshing surface friction heat flow, and has decisive influence on gear teeth bulk temperature (Marciano *et al.* 2010, Bendavid *et al.* 2010, Mo *et al.* 2009, Mo and Szlufarska 2010). Considering traditional

calculation method cannot accurately determine real stress distribution and deformation (Yang and. Martini 2013, Mishra and Szlufarska 2012, Mishra *et al*. 2012, Yang and Martini 2013).

In order to understand the mechanism of thermodynamic contact status and coupling effects of gear pairs meshing state in the operation process, in the study, research and analysis on thermodynamic coupling according to teeth temperature field, displacement field and stress field of the gear system. The results of load deformation and contact strength have a theoretical significance in research warship gear system.

2. The tribo-dynamics model

In order to obtain the closed-form representation of the teeth surface, a geometric meshing theory is presented by combining a simplified equation of meshing with the geometric equation. The simplified equation of meshing is introduced by applying the vector form representation of the surface revolution to the equation of meshing, and then the geometric meshing theory is given as follows.

Assume that the motion parameter of the generating process is ϕ, and then Eq. (1) can be formulated

$$r(h,\theta,\phi) = o(\phi) + h \cdot l(\phi) + \rho(h) \cdot n(h,\theta,\phi) \tag{1}$$

Where, the parameter ϕ is the velocity of the generating surface can be formulated

$$v(h,\theta,\ \phi) = \frac{do(\phi)}{d\phi} + h \cdot \frac{dl(\phi)}{d\phi} + \rho(h) \cdot \frac{\partial n(h,\theta,\ \phi)}{\partial\phi} \tag{2}$$

Considering Eq. (1) and Eq. (2), then can be formulated

$$n \cdot v = n(h,\theta,\phi) \cdot \left[\frac{do(\phi)}{d\phi} + \frac{dl(\phi)}{d\phi} \right] \tag{3}$$

Considering Eqs. (1)-(3) can be rewritten as

$$\rho h = o + h \cdot 1 \tag{4}$$

Where, ρh is the position vector.

Following Eq. (3), Eq. (4) can be rewritten as

$$\rho h(\phi) = o(\phi) + h \cdot 1(\phi) \tag{5}$$

The tangential velocities of the tooth flanks produce the effective. These velocities are variable along the line of action, with the constant angular velocities of the driving and driven gear wheels, respectively, are defined using the following equations

$$v_h(h,\phi) = \frac{do(\phi)}{d(\phi)} + h \cdot \frac{dl(\phi)}{d(\phi)} \tag{6}$$

$$n(h\theta\phi) \cdot v\,h(h\phi) = 0 \tag{7}$$

Where, vh is the position velocity vector.

In the calculation model, Eq. (7) means that if ρ is a contact point, the normal of the generating surface at ρ is orthogonal to the velocity of the generating surface at ρh. The variable load is produced by the alternating meshing of several pairs of teeth. When gear pairs practically designed, normally alternate between single and double meshing. A special characteristic of the meshing equation for the generating surface is a surface of revolution. Another important feature of Eq. (7) is that vh is not related with the parameter θ, and this is helpful to represent the contact point as a closed-form expression in any chosen coordinate system.

In this paper, when defining the structural material characteristics and the addition thermal expansion coefficient, the program selection with the same node structure unit of plane 42 and solid 45, the temperature field unit of plane 55 and solid 70. In the thermodynamic coupling analysis, node temperature obtained by solving the temperature in structural analysis as body load applied on the corresponding node.
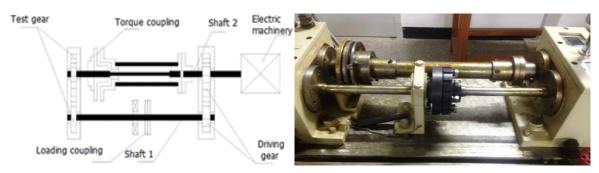
3. Experimental

3.1 Experimental setup

In this work, closed power-flow gear transmission testing bed (CPF) was used to conduct the tests. The CPF test bed is shown in Fig. 1. There were two pairs of spur gears including one pair of tested gears and one pair of driving gears.

In this test bed, torque coupling was employed to obtain the torque load. A detachable lever was attached on the torque coupling, and then dead loads were applied on the lever to produce the load. The product of the lever length and the dead load was the torque load on the spur gears. The design of test bed was ideal for our tests because it can change the load and speed of spur gears easily to investigate their effects on TCA.

3.2 Gears parameters

Basic parameters of tested gears were presented in Table 1.

(a) Schematic of experimental setup   (b) Real experimental setup

Fig. 1 Schematic of experimental setup and real experimental setup

Table 1 Parameters of tested gears

Teeth form number	1	2
Number of gear teeth, z_1 and z_2	18	36
Normal module, (mm)	3	3
Teeth width, (mm)	50	50
Pressure angle, (degree)	20	20
Driving gear speed, n_1 (r/min)	2000	
Load factor, k	1.3	
Power, p (kW)	9000	
Young's modulus, E_1 and E_2 (GPa)	206	

Table 2 Material properties

Poisson's ratio, μ_1 and μ_2	0.26
Thermal conductivity, k_1 and k_2 (W/m·K)	46
Density, ρ_1 and ρ_2 (kg/m^3)	7850
Heat capacity, c_1 and c_2 J/(kg·K)	470

Test gears are made of SAE8620 steel, which has a hardness of 55 HRC. And gear surface roughness is 1.6-3.2 μm for all tested gears. The material properties of tested gears have been presented in Table 2.

3.3 Lubricating oil

In this section, tested gears were lubricated using oil splashing method. The oil was heated until the temperature reached 95℃ in an oil depot where the heater and thermostat were installed. Lubricating oil was pumped at a constant flow rate of 2.4 L/min from the nozzle to meshing point of tested gears on their engaging side. Material properties of lubricant were presented in Table 3.

Table 3 Material properties of lubricant

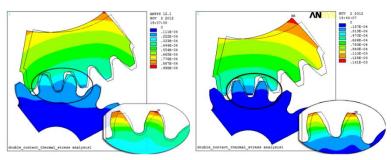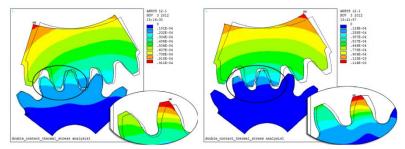| Viscous pressure coefficient, α (m^2/N)	2.2×10^{-8}
Oil steady state temperature, T_0 (K)	343
Initial viscosity, η_0 (Pa·s)	0.034
Initial density, ρ_0 (kg/m^3)	884
Thermal conductivity, K W/(m·K)	0.14
Specific heat capacity, c J/(kg·K)	2129.87

4. Simulation results

4.1 TCA of spur gear

In order to obtain the stress situation of engagement gear in the whole process must calculate the stress of plurality engagement position. This paper focuses on calculating the stress state of several key engagement positions, considering the whole meshing process at least two pairs teeth in mesh, at the junction of two and three teeth meshing area, teeth surface load greater, the contact stress will greatly change.
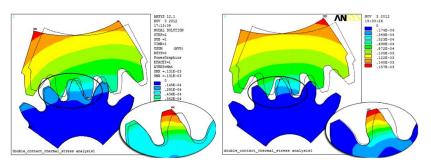
By changing the position of engagement angle, on driving wheel to rotate 35 degrees stress range, selected 16 meshing position of contact analysis. Different meshing angle gear deformation in Fig. 2. Different meshing angle gear stress in Fig. 3.
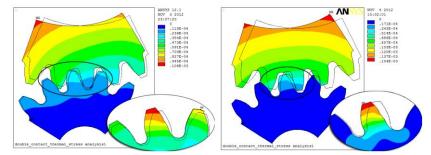

Position 1: rotation angle 1, mesh node number 222, number of nodes from addendum 0
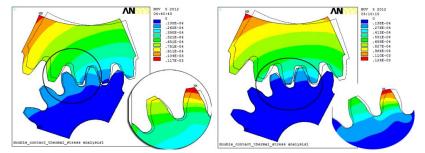

Position 2: rotation angle 15.5, mesh node number 253, number of nodes from addendum 33

Position 3: rotation angle 17.5, mesh node number 256, number of nodes from addendum 36
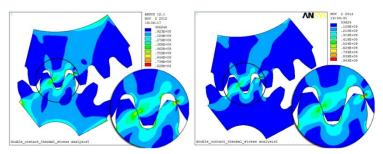
Continued-

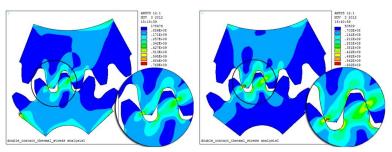Position 4: rotation angle 20.5, mesh node number 249, number of nodes from addendum 40

Position 5: rotation angle 35, mesh node number 234, number of nodes from addendum 55
(Left are TCD nephogram, Right are Elastic deformation nephogram)
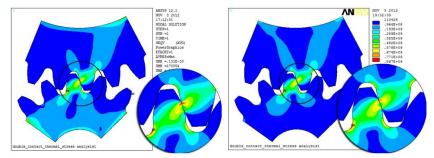
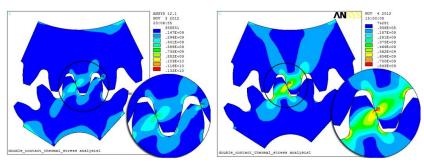Fig. 2 Different meshing angle gear deformation

Position 1: rotation angle 1, mesh node number 222, number of nodes from addendum 0
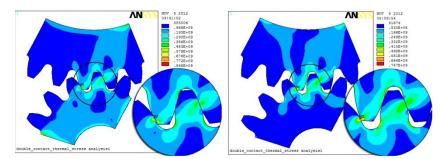

Position 2: rotation angle 15.5, mesh node number 253, number of nodes from addendum 33
Continued-

Position 3: rotation angle 17.5, mesh node number 256, number of nodes from addendum 36

Position 4: rotation angle 20.5, mesh node number 249, number of nodes from addendum 40

Position 5: rotation angle 35, mesh node number 234, number of nodes from addendum 55
(Left are TCCS nephogram, Right are Elastic contact stress nephogram)

Fig. 3 Different meshing angle gear stress

From Figs. 2 and 3 seen, when single teeth meshing to prepare double teeth position, rotation angle 20.5, number of nodes from addendum 40. When the single teeth just to double teeth meshing, this is the calculation of driven gear teeth tip modification position. When the single teeth meshing is just ready to engage out, this is the calculation of driving gear teeth tip modification position. Then thermal deformation analysis (TDA) of spur gear.

4.2 TDA of spur gear

Thermodynamic deformation (TD) model and contact stress in Fig. 4, Elastic deformation (ED) model and contact stress in Fig. 5, Driven gear elastic deformation in Fig. 6, Driven gear thermal expansion in Fig. 7, Driving gear elastic deformation in Fig. 8.
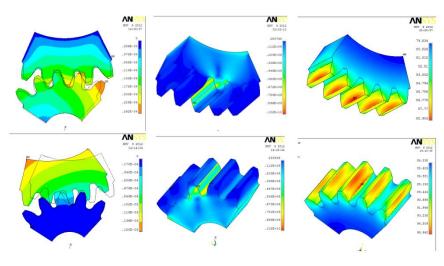

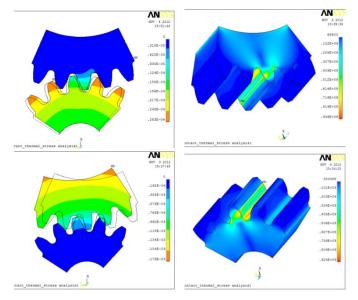Fig. 4 Thermodynamic deformation model and contact stress

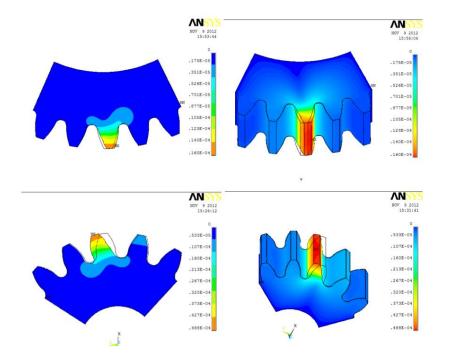Fig. 5 Elastic deformation model and contact stress

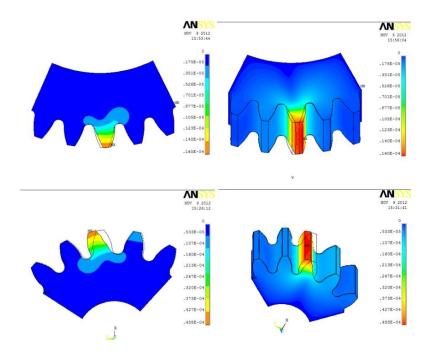Fig. 6 Driven gear elastic deformation

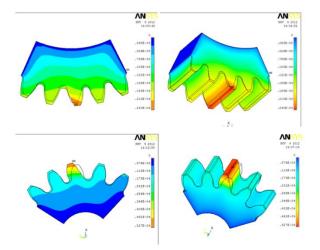
Fig. 7 Driven gear thermal expansion
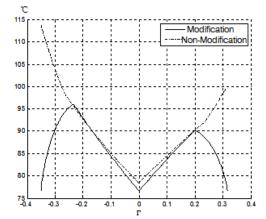
Fig. 8 Driving gear elastic deformation

Fig. 9 Spur gear along meshing line modification temperature contrast

From Figs. 4-7 seen clearly, as the influence of gear teeth stiffness and thermal deformation, resulting in gear teeth thickness becomes larger; the maximum thermal deformation appeared in the addendum. From Fig. 8 seen clearly, after thermal deformation gear teeth become higher, the whole teeth are relatively larger; the calculated thermal deformation is 15.6 μm.

4.3 Case study

This paper proves that due to the presence of elastic deformation and thermal deformation, gear meshing impact cause stress concentration, which proves the necessity of gear modification. According to the thermal elastic deformation for gear calculation with modification curve formula, obtained the desired thermal elastic deformation, based on gear modification curve, and provide theoretical basis for the further study on the influence of friction heat flow on gear teeth surface.
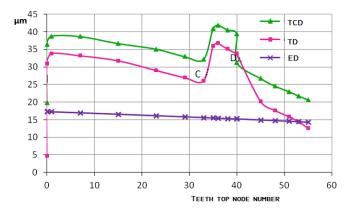
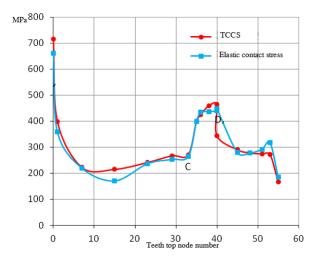Fig. 10 Each point of meshing line deformation

Fig. 11 Each point contact stress of the meshing line

Spur gear along meshing line before and after modification temperature contrast in Fig. 9.

From the Fig.9 seen, the trend of temperature distribution along meshing line and ISO standard is same, according to TCA requires modification.

5. Experimental results and discussion

According to TCA results of modified spur gears influence on thermal elastohydrodynamic lubrication characteristics are discussed. By comparing the whole meshing teeth deformation of 2D curve, thermal elastic deformation and elastic deformation of the same tendency, the former than the latter is higher than a certain value, the thermal deformation is nearly constant, the FEM

results with similar theory. Each point of meshing line deformation in Fig. 10.

The gear teeth bending deformation caused by the contact stress, in this section, two pairs of spur gears are used to investigate their TCD using the present method. Each point contact stress of the meshing line in Fig. 10.

From Fig. 11 contact stress curve can be found, when gear pairs will recess contact, its stress swells.

6. Conclusions

In this work, calculation on elastic analysis and thermo elastic coupling of spur gear pairs under meshing conditions. The conclusions can be drawn as follows:

In a cycle of gear meshing, analyzed every rotating an angle gear contact stress, elastic deformation, thermodynamic coupling contact stress and thermal elastic deformation.

Compared of the change rules, from the curve view, when the single teeth entering meshing and disengaging meshing, contact stress and thermal elastic deformation amount is maximum.

Demonstrated that due to the presence of elastic deformation and thermal deformation gear meshing impact cause stress concentration, which proves the necessity of gear modification.

Obtained the desired thermal elastic deformation, based on gear modification curve, provide theoretical basis for the further study on the influence of friction heat flow on gear teeth surface.

Acknowledgments

References

Bendavid, A., Martin, P.J., Randeniya, L., Amin, M.S. and Rohanizadeh, R. (2010), "The properties of fluorine-containing diamond-like carbon films prepared by pulsed DC plasma-activated chemical vapour deposition", *Diamond Relat. Mater.*, **19**, 1466-1471.

Czichos, I.H. (2010), *Tribologie-Handbuch*, (3th Ed.), Praxis, Berlin.

De Mello, J.D.B., Binder, R., Demas, N.G. and Polycarpou, A.A. (2009), "Polycarpou. Effect of the actual environment present in hermetic compressors on the tribological behaviour of a Si-rich multifunctional DLC coating", *Wear*, **267**, 907-915.

De Mello, J.D.B., Binder, C., Hammes, G. and Klein, A.N. (2013), "Effect of the metallic matrix on the sliding wear of plasma assisted debinded and sintered MIM self-lubricating steel", *Wear*, **301**, 648-655.

Efremov, E.V., Ariese, F. and Gooijer, C. (2008), "Achievements in resonance Raman spectroscopy review of a technique with a distinct analytical chemistry potential", *Anal. Chim. Acta.*, **606**, 119-134.

Escobar Galindo, R., Gago, R., Albella, J.M. and Lousa, A. (2009), "Comparative depth-profiling analysis of nanometer-metal multilayers by ion-probing techniques", *TrAC Trends Anal. Chem.*, **28**, 494-505.

Hammes, G., Schroeder, R., Binder, C., Klein, A.N. and de Mello, J.D.B. (2014), "Effect of double pressing/double sintering on the sliding wear of self-lubricating sintered composites", *Tribol. Int.*, **70**, 119-127.

Hanesch, M. (2009), "Raman spectroscopy of iron oxides and (oxy) hydroxides at low laser power and possible applications in environmental magnetic studies", *Geophys. J. Int*., **177**, 941-948.

Gayathri, S., Kumar, N., Krishnan, R., Ravindran, T.R., Dash, S. and Tyagi, A.K. *et al.* (2012), "Tribological properties of pulsed laser deposited DLC/TM (TM=Cr, Ag, Ti and Ni) multilayers", *Tribol. Int*., **53**, 87-97.

Kim, H.K., Park, S.H., Lee, H.G., Kim, D.R. and Lee, Y.H. (2007), "Approximation of contact stress for a compressed and laterally one side restrained O-ring", *Eng. Fail Anal*., **14**(8), 1680-1692.

Marciano, F.R., Almeida, E.C., Lima-Oliveira, D.A., Corat, E.J. and Trava-Airoldi, V.J. (2010), "Improvement of DLC electrochemical corrosion resistance by addiction of fluorine", *Diamond Relat. Mater*., **19**, 537-540.

Mironova-Ulmane, N., Kuzmin, A., Steins, I., Grabis, J., Sildos, I. and Pärs, M. (2007), "Raman scattering in nanosized nickel oxide NiO", *J. Phys. Conf. Ser*., **93**, 012039.

Mishra, M. *et al.* (2012), "Friction model for single-asperity elastic-plastic contacts", *Phys. Rev. B: Condens. Matter*., **86**, 4.

Mishra, M. and Szlufarska, I. (2012), "Analytical model for plowing friction at nanoscale", *Tribol. Lett*., **45** (3), 417-426.

Mo, Y.F., Turner, K.T. and Szlufarska, I. (2009), "Friction laws at the nanoscale", *Nature*, **457**(7233), 1116-1119.

Mo, Y.F. and Szlufarska, I. (2010), "Roughness picture of friction in dry nanoscale contacts", *Phys. Rev. B: Condens. Matter*., **81**, 3.

Nikas, G.K. (2010), "Eighty years of research on hydraulic reciprocating seals: review of tribological studies and related topics since the 1930s", *Proceedings of the Inst. Mech. Eng. Part J J Eng Tribol*., **224** (1), 1-23.

Radhika, R., Kumar, N., Kozakov, A.T., Sankaran, K.J., Dash, S. and Tyagi, A.K. *et al.* (2014), "Role of transfer layer on tribological properties of nanocrystalline diamond nanowire film sliding against alumina allotropes", *Diamond Relat. Mater*., **48**, 6-18.

Rout, T.K. (2007), "Nanolayered oxide on a steel surface reduces surface reactivity: Evaluation by glow discharge optical emission spectroscopy (GDOES)", *Scripta Mate*r., **56**(7), 573-576.

Silverio, M., Binder, R. and De Mello, J.D.B. (2011), "Estudo Tribológico de Revestimentos de DLC Com Gases Refrigerantes HFC134A e HC600A", *Tecnolem. Metale. Mater*., **8**, 64-72.

Wilke, M., Teichert, G., Gemma, R., Pundt, A., Kirchheim, R. and Romanus, H. *et al.* (2011), "Glow discharge optical emission spectroscopy for accurate and well resolved analysis of coatings and thin films", *Thin Solid Films*., **520**, 1660-1667.

Yang, B., Salant, R.F. and Soft, E.H.L. (2009), "Simulations of U-cup and step hydraulic rod seals", *J. Tribol. – T. ASME*, **131**(2), 02150.

Yang, L. and Martini, A. (2013), "Nano-scale roughness effects on hysteresis in micro-scale adhesive contact", *Tribol. Int*., **58**, 40-46.

Yang, L.Q. and Martini, A. (2013), "Nano-scale roughness effects on hysteresis in micro-scale adhesive contact", *Tribol. Int*., **58**, 40-46.

Zhang, Y.S., Han, Z. and Lu, K. (2008), "Fretting wear behavior of nanocrystalline surface layer of copper under dry condition", *Wear*, **265**(5-8), 396-401.